Dual Polarization Interferometry: A Real-Time Optical Technique for Measuring (Bio)molecular Orientation, Structure and Function at the Solid/Liquid Interface

CHAPTER · MARCH 2008

DOI: 10.1002/9780470061565.hbb055

3 AUTHORS, INCLUDING:

Graham Hugh Cross
Durham University
96 PUBLICATIONS **1,406** CITATIONS
SEE PROFILE

Marcus Jack Swann
Swann Scientific Consulting Ltd.
73 PUBLICATIONS **1,636** CITATIONS
SEE PROFILE

32

Dual Polarization Interferometry: A Real-Time Optical Technique for Measuring (Bio)molecular Orientation, Structure and Function at the Solid/Liquid Interface

Graham H. Cross,[1] Neville J. Freeman[2] and Marcus J. Swann[2]

[1] Department of Physics, Durham University, Durham, UK and [2] Farfield Scientific Ltd., Crewe, UK

1 INTRODUCTION

The challenging task of understanding and measuring the function of proteins and other biological molecules in all their structural and environmental complexity is one that has spawned a myriad of different techniques in the field of biological sciences. These span those providing exquisite detail in terms of molecular structure of a static system, such as X-ray crystallography or neutron reflection, to those providing dynamic measurements of protein function such as protein–protein interaction kinetics measured by some of the biosensing techniques covered in this handbook. Such measurements provide pieces of a jigsaw puzzle which need to be combined with others to provide a full picture. Of course, the function of any (bio)molecule is critically dependent on its environment, structure, and molecular arrangement. As such the ability to provide information linking these different areas is of fundamental interest.

Here we look at one such technique, dual polarization interferometry (DPI). This optical, surface analytical technique provides a multiparametric measurement of molecules at a surface to give information on molecular dimension (layer thickness) and packing (layer refractive index (RI), density) and surface loading and stoichiometry (mass). This combines the analytical nature of neutron reflection with the real-time, bench-top accessibility associated with biosensors and can be used to provide a link between a molecule's structure and its function.

This chapter puts DPI in the context of other multiparametric optical techniques, outlines the principles behind the technology and its implementation together with some simple examples to provide validation of the measurement. The basic experimental and data analysis methods are covered together with examples of areas of application of the technology specifically where structural information complements more conventional "mass" dependent measurement.

Handbook of Biosensors and Biochips. Edited by Robert S. Marks, David C. Cullen, Isao Karube, Christopher R. Lowe and Howard H. Weetall.
 ISBN 978-0-470-01905-4.

The growth, metabolism, and replication of cells, the basic building blocks of life, depend very heavily on proteins. Proteins, while expressed within the cells themselves, perform a vast range of functions of both an intracellular and intercellular nature. The profile of expressed proteins within a cell depends upon the metabolic status of the cell, its age, and its local environment. Understanding the role that proteins play in the status of the cell is crucial to the understanding of the diseased state and is therefore of great importance within medical and pharmaceutical studies of disease.

In order to understand the complex nature of protein function and the many different roles a protein may have, real-time measurements of proteins and their behavior is required.

The structure of a protein is determined by its primary, secondary, and tertiary structures, the latter two being noncovalent in nature and a range of interactions contribute to the final structure such as hydrogen bonding, electrostatic interactions, and dispersion forces. These interactions occur between adjacent amino acid groups and may be mediated or altered by solvation, the ionic strength of the solution, and a range of other environmental factors such as pH or temperature. Measurement of the dimensions of a protein layer as a function of these variables can probe these factors, and a particular protein's sensitivity. The dynamic nature of the secondary and tertiary structures of proteins enables them to undergo structural changes in response to stimuli which are often related to their functional roles. Structurally distinct regions within a protein are often associated with specific functions and these structures may be conserved to undertake similar functions across a range of different proteins. Finally, these individual peptides often interact with other peptides to perform specific functions or to provide structural integrity and this final structure of the protein is known as the *quaternary structure*.

The shape of the protein, especially its external surface often provides pockets or clefts, which offer specific binding sites for small molecules or other proteins. Interaction with these sites is often described as "specific binding" and is associated with the activation or regulation of the activity of the protein.

Probing the dimensional aspects of these interactions with other proteins, peptides, and other ligands and small molecules can provide information about the specific nature of the interactions. For example, determining how the layer structure of an oriented immobilized protein changes on binding its partner can indicate the location on the protein at which the binding site resides.

Indeed for protein–small molecule complexes, interactions can be dominated by structural or conformational changes. This is particularly relevant to the pharmaceutical industry. Small molecules may interact in a range of ways with a protein, dependent on the nature and number of the binding sites. Determining a structural signature for a small molecule binding can differentiate between different modes of interaction. These may include molecules binding to the same site with different degrees of specificity, whether they promote a specific conformational change or not and those binding to unrelated sites.

The behavior of proteins at interfaces (e.g., surfaces) is of particular relevance. The first aspect of this, is that many biologically important processes are interfacial in nature, with for example, the interaction of molecules at membrane surfaces whether above, within, or across the membrane bilayer. Lipid layers and vesicles can be immobilized and quantified and their interactions then probed through both mass and structural changes.

The second aspect relates to the many of the ways we use proteins, many of which require us either to immobilize them or to prevent them from being immobilized at a surface. So following the structural evolution during the construction of a protein surface to be used for example, as a diagnostic test can help understand the factors influencing the functioning or otherwise of the proteins within the immobilized assembly. Alternatively, the detailed characterization of a surface and its interaction with proteins can be a valuable tool to understand the mechanisms of biofouling or protein resistant surfaces.

2 TECHNOLOGY

2.1 Overview of Optical Techniques

Spectroscopic ellipsometry is the most familiar method by which the optogeometrical properties of thin films may be deduced.[1,2] This technique analyzes the state of polarization of light reflecting from multilayer reflective samples and

uses the laws of electromagnetism (formulated as Maxwell's equations applied to reflection and refraction at the layer interfaces) to resolve the layer thicknesses and RIs of the layers. The analysis requires the experimenter to choose a specific structural model from which the corresponding expected data may be calculated and to which the observed data may be compared via an error minimization process. There is, alongside this, an increasing interest in optical-guided wave techniques that are able to determine the average thickness and density of ultrathin layers that bind to an optical waveguide surface.[3–6]

In any optical waveguide structure, the light field is not wholly confined within the physical boundaries of the guiding medium but, rather, decays exponentially away from the boundaries. This part of the optical field is known as the *evanescent* (*vanishing*) *field*. If a layer is added to or removed from the original waveguide surface or an existing layer changes its thickness or density the position of the boundary at which the light begins this exponential decay is altered. Such changes alter the speed of propagation ("phase velocity") of the whole field. Here, the measured changes to the phase velocity of optical fields probing the layers are interpreted through application of Maxwell's equations to guided optical fields in multilayer samples. These developments follow on from the widely used and commercialized evanescent wave methods, notably surface plasmon resonance (SPR) spectroscopy,[7,8] where the information provided is limited to the change in a mass-related parameter (resonance angle shift) at the optical surface as a function of time. Thus the measurement of the kinetics of molecular binding events (association and dissociation constants) and concentration measurements have been the two main applications for evanescent wave sensors until recently.

While there is still a great need for such simple information obtained with the speed and sensitivity that evanescent wave methods offer, the variety of examples given in the preceding text require a greater degree of information to distinguish different possible behavior of the proteins being studied. Structural changes have been inferred from single parameter measurements, as for example, the observed "mass" response will be enhanced or suppressed by the effect of the conformational change. This can only be interpreted however with a view to what the expected mass change should have been and there are too many potential contributions from other factors to make this a viable approach in general. Most instances can be attributed to effects such as binding-promoted surfactant adsorption/desorption or ion motion due to pI changes of the protein or related immobilization matrix effects. In short, a single measurement by evanescent wave techniques cannot be interpreted for layer structure with any confidence without some additional information.

With low noise instrumentation, evanescent wave techniques have the capability to resolve layer dimensional changes at the sub-angstrom level and RI increments of 10^{-6}.

Here we describe methods that use an additional independent evanescent wave measurement to remove these ambiguities (dual mode evanescent wave spectroscopy (DMEWS)). With dual mode evanescent wave methods, the capability inherent in spectroscopic ellipsometry is shared by the guided wave techniques, the layer model assumptions are similar but the methods of data analysis are distinctly different. While in ellipsometry the data is analyzed using a multiparameter model fit using the χ^2 statistic and its minimization, in guided wave methods the phase velocity change data is carried through directly to the layer parameters required to produce such a change. It will be important to remember however that all methods require the correct choice of model in order to be successful.

We will concentrate on the experimental determination of the two optogeometrical parameters (average RI and thickness) of a uniform, isotropic thin film: In ellipsometry, the corresponding model system is a "three-phase" model.[1,2] In an optical waveguide measurement we need two independent sources of experimental data. These might comprise a data pair taken from two evanescent fields at different optical wavelengths or, to reduce the uncertainty that optical dispersion might introduce two orthogonally polarized fields at a fixed wavelength. Although there are developments possible with the former, we will concentrate on the application of the latter method. Here one can distinguish between methods that rely on the measurement of modal phase matching conditions (resonance techniques) and reflectometry, and that implemented in DPI which relies on the interferometric detection of optical field phase changes.

In the coupled plasmon waveguide resonance (CPWR) technique[9] the waveguide structure comprises a Kretschman-type SPR arrangement[10] but with the addition of a thin low RI dielectric film (silicon dioxide) above the silver film. As in conventional SPR the interface between the metal and the emergent dielectric confines an optical field with transverse magnetic (TM) polarization. Light incident through the coupling prism is therefore polarized in the plane of incidence ("p" polarized.) However, this simple layer addition allows the combined system to also confine a transverse electric (TE) field which can be coupled to by incident light polarized orthogonal to the plane of incidence ("s" polarized). Each of the two modes has an electric field component (the evanescent field) whose amplitude decays exponentially, but at different rates, beyond the dielectric layer into the medium of interest.

In experiments the incidence angle is scanned with high angular resolution and the reflected light intensity is measured around a range of angles spanning the angles of minimum reflection. At these coupling angles, the tangential phase velocity of light in the prism matches that of the waveguide field and the real part of the effective index of the structure may be related to the angle. Thus as layers are added to the system this "phase matching" condition changes and the resonance angle changes.

From a full analysis of data taken from the reflection spectrum it is, in principle, possible to use transfer matrix methods[11] and multiparameter fitting procedures to give the layer thickness and the RI and extinction coefficient for each of the two polarizations. One important example where this has been applied is to lipid bilayer systems where the optical properties normal to the bilayer are distinctly different to those in the layer plane.[5]

In optical waveguide light mode spectroscopy[12,13] (OWLS), the waveguide structure is a simple slab waveguide into which light may be coupled using a grating to achieve phase matching. As in all such coupling methods, light entering the structure must have a tangential phase velocity (determined by coupling angle) equal to that of the optical waveguide field. The dielectric slab waveguide is designed to support fields (or "modes" from hereon) of each polarization, TE, and TM. At an appropriate angle of incident light when the phase matching condition is achieved, the waveguide mode is excited and propagates light along to the waveguide end facet where it is collected by a photodiode and recorded. These angles will change according to changes above the original surface as described earlier. Since the TE and TM resonance angles are separated from each other, it is difficult to implement a system that can track the resonance minima of two such modes in real time. Thus for real-time studies the technique works by following the shift in resonance angle for a single polarization. Kinetic studies are therefore possible. The layer optogeometrical properties can however be extracted after the layer has bound by measuring the resonance shifts for both polarizations individually. These will provide the effective index changes for TE and TM polarized modes and using numerical solution of the eigenvalue equations for the waveguide system and making the assumption that the only unknown layer is uniform and isotropic its thickness and index can be found. In cases where this assumption is not strictly valid the thickness and RI data will have inaccuracies and the extent to which these might be introduced in OWLS and other studies has been examined by Mann.[14]

2.2 Dual Polarization Interferometry (DPI)

Interferometers comprise devices with two optical paths that detect the change in optical path length experienced by an optical field passing through the sensing path of the interferometer. Sensitivity is governed by, among other things, the interaction length and the signal-to-noise ratio of the detection scheme. Typically, integrated optical interferometers are configured in the Mach–Zehnder format[15] by creating channel waveguiding regions in the top surface of an optical dielectric stack. DPI uses a much-simplified interferometer based on slab waveguides, with the reference slab waveguide buried beneath the sensing waveguide simply as part of the multilayer fabrication process (see Figure 1a).

Coherent light broadly illuminates the stack end facet, exciting all possible modes (guided and radiation) in the structure but only the guided modes propagate more than 50 μm or so along the path.[16] Upon exiting the structure (after 20 mm or so depending on sample length) the light from the two modes diffracts into free space. Because the

waveguides are so close together (only ~4 μm apart) the diffracted wavefront generates the well-known pattern of Young's interference fringes in the far-field only a few millimeters from the end facet. Changes in the optical properties of the sensing waveguide (e.g., layer changes) translate into variations in the phase of the sensing mode field and then into interference pattern intensity shifts, as captured by a high-resolution camera. The optical tolerances are so forgiving that macroscopic movements of the input coupling beam on the order of hundreds of micrometers cause no change in the interference pattern. These loose tolerances allow the stack to be inserted and removed from the optical train without precision alignment, an essential characteristic for a disposable measurement platform. The waveguide stack is designed so that both measurement and reference arm support single modes in both TE and TM polarizations, enabling two optical phase change measurements to be made and the polarization of the light is alternately switched on a 2-ms cycle using a ferroelectric liquid crystal rotator.

Direct measurement of the phase change is obtained by continuously monitoring the relative phase position of the fringe pattern by performing

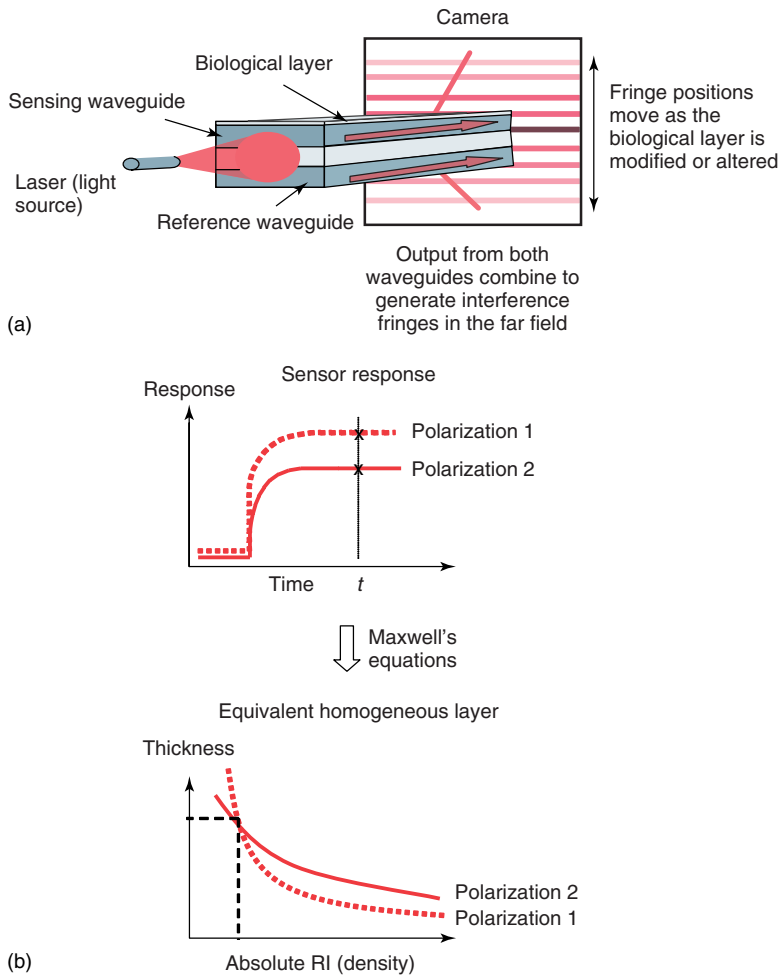

Figure 1. (a) Schematic diagram of a laser illuminated measurement chip, with fringes produced on the camera as the propagated light diffracts out of the end of the waveguides and interferes. [Reprinted with permission M J Swann et al., copyright 2004, Elsevier.] (b) Schematic diagram of the process of conversion of measured phase data to calculated layer thickness and refractive-index values. [Reprinted with permission from Farfield Scientific Ltd.]

a Fourier transformation relating intensity to position. The application of a standard transfer matrix approach provides evaluation of the guided modes for the structure. This allows inclusion of an arbitrary number of layers in a model, each of which is represented by its own layer matrix. Calibration of the bare chip using two liquids of known RIs as upper layers to generate TE and TM phase changes provides an initial structure (waveguide layer thicknesses and indices.) A successive approximation method provides the optimum refractive-index value and the thickness of the waveguide layer. Subsequent phase changes are analyzed similarly by including a model uniform isotropic thin layer on the surface of the waveguide (see Figure 1b) and resolving its properties (index and thickness). This calculated layer corresponds to the single homogeneous layer equivalent to the layer deposited experimentally. The layer density can be determined from the RI (see subsequent text) and knowing size and density, one can also trivially calculate the total mass, surface concentration, number of protein molecules, molecular footprint, and other useful parameters.

Because experimentally, layers of different proteins or other materials can be deposited sequentially, it can sometimes be the case that a layer has been deposited which is not expected to change during the ongoing course of the experiment. This layer can then be incorporated as a fixed layer in the optical multilayer structure, and subsequent changes calculated as a new layer on top. Where this analysis does not produce realistic results, this can indicate the subsequent layer is either penetrating or expanding the sublayer.

Where the assumption of a uniform isotropic layer is not valid alternative approaches can be used and have been applied successfully, for example, to lipid bilayer systems.

2.3 Experimental Setup

The measurement chip is located on a thermal block which is held at the preset temperature of between 10 and 40 °C with a stability of ±2 mK. The illumination is provided by a 632.8 nm He–Ne laser. Running buffer or samples are exposed to the two fluidic channels of the measurement chip via a fluidic manifold supplied by an high pressure liquid chromatography (HPLC)-type sample injection system driven by a syringe pump. The fluidics can be configured to allow a variety of sample volumes and viscosities to be introduced, and the sample flow may be maintained or stopped to allow samples to incubate on the chip surface. While experiments are generally undertaken in aqueous phase, most water miscible solvents can be used. The RI range for the running buffer is 1–1.49. For thin layers however there is no upper limit on the layer RI.

Measurement chips are calibrated at the beginning of a measurement with solutions of known RI, typically 80% ethanol/water and pure water. This allows the sensitivity of the phase response and hence waveguide parameters to be calculated. Measurement of the phase change between the water and the running buffer also allows the RI of the buffer to be checked. These values are then used for the chip structure in the subsequent data analysis.

2.3.1 Typical Experimental Approach

Experiments usually start from either an unmodified silicon oxynitride chip, or using one that has been chemically modified with an alkoxysilane (mono)layer. Typical surface functionalities are amine, thiol, or hydrophobic—either trimethylsilane or octadecylsilane, from which a variety of immobilization methodologies may be employed.

Proteins may be physisorbed, either via hydrophobic, hydrophilic, or electrostatic interaction, or can be coupled to the surface with a cross-linker. This may be direct covalent coupling with a bifunctional cross-linker, or via an intermediate coupling layer, such as via biotinylation of an amine chip, coupling of streptavidin followed by binding of a biotinylated protein.

As much of the protein layer immobilization as possible is generally undertaken on the instrument this ensures that all layers can be properly quantified and the final surface structure can be accurately calculated from the measured phase shift starting from the initial bare or modified surface. Once the layer thickness and RI have been measured, values for the protein layer density, mass, molecular footprint and so on, can be calculated.

2.3.2 Typical System Performance

Experimentally observed errors are somewhat dependent on the nature of the layers being measured. For a typical protein monolayer the errors are shown in Table 1. In thickness the resolution equates to less than one-tenth of an atomic bond length. Where layers are very diffuse, or the layer thickness approaches the $1/e^2$ extent of the original evanescent field ($\sim$100 nm for an aqueous system with layer RI < 1.40) these may be larger.

2.4 Data Analysis

The RI increments of proteins are quite consistent[1,17,18] with typical values in the region of 0.186 g cm^{-3} and it is therefore possible to determine the mass of material deposited on the sensor surface in a similar way to that of de Feijter[19] using equations (1) and (2)

$$\rho_L = \frac{\rho_p(n_L - n_s)}{(n_p - n_s)} \quad (1)$$

$$m_L = \rho_L \tau_L \quad (2)$$

where ρ_L is the adsorbed layer density, ρ_p is the protein density, n_L is the adsorbed layer RI, n_p is the protein RI, n_s is the solution (bulk) RI, m_L is the mass loading per unit area, and τ_L is the adsorbed layer thickness.

From the mass loading it is straightforward to calculate the area per molecule according to equation (3)

$$A = \frac{M_w}{N_a m_L} \quad (3)$$

where A is the area per molecule, M_w is the protein molecular weight, and N_a is Avogadro's number.

By using the measured values for the RI of the bulk solution the volume fraction of the layer occupied by protein (ϕ_p) can also be calculated using equation (4):

$$\phi_p = \frac{(n_L^2 - n_s^2)}{(n_p^2 - n_s^2)} \quad (4)$$

After calculation of the parameters described in the preceding text, it is possible to draw inferences not only regarding the gross structures of the deposited protein layers but also the likely orientation of the protein molecules within the layers.

2.5 Measurement Validation and Model Examples

Validation of the measurements has been made using a variety of methods, generally however the use of measurements of protein dimensions as a validation methodology should be used with caution, as proteins may conform significantly onto solid surfaces and this degree of deformation can itself be a function of protein surface loading. Comparative measurements of protein systems against other techniques have been made. cf. C receptor protein as a comparison with atomic force microscopy (AFM),[20] bovine serum albumin (BSA) structures as compared with neutron reflection[21] or streptavidin immobilized on a biotinylated surface[22] and an antibody oriented on a protein G surface (shown subsequent text) compared with its X-ray crystallographic dimensions. In the two latter cases, where the comparative technique (X-ray crystallography) is not a surface method, the proteins are captured via a specific interaction which means that both are specifically

Table 1. Typical percentage CV in phase, temperature, and "resolved" layer values from DPI measurements

Parameter	Typical layer value	Accuracy (±)	Resolution (±)
TM phase measurement	8 rad	0.25%	0.8 mrad (0.01%)
Mass (ng mm^{-2})	2 ng mm^{-2}	<1%	0.2 pg mm^{-2} (0.01%)
Thickness	5 nm	5%	0.01 nm (0.2%)
Density	0.4 g cm^{-3}	5%	0.0004 g cm^{-3} (0.2%)
Temperature	20 °C	0.1 K	2 mK

[Reprinted with permission from Farfield Scientific Ltd.]

oriented and also reduces the likelihood of deformation of the protein at the surface.

Verification using well-defined nonprotein systems has used polymer layers or particulate adsorption. Comparisons using polymer multilayer deposition has been made to good effect, with dimensional measurements providing reasonable values from the very first layers at the nanometer level (where ellipsometry is not so reliable) to much thicker layers in the tens of nm and beyond, which agree very closely with values measured via ellipsometry.[23]

2.5.1 Nanospheres

One example of measurements of a nonconformable particle is that of carboxylated polystyrene nanospheres. The spheres are available in a range of sizes (Invitrogen, Molecular Probes) and are negatively charged, and so physisorb via electrostatic interaction onto an amine functionalized chip surface in phosphate buffered saline solution (PBS). The packing density of the spheres can be varied by changing the pH of the experiment. The high charge on the spheres means that at pH 7.4 sphere–sphere repulsion limits the surface coverage, which increases as the pH is lowered. Figure 2 shows a plot of measured layer thickness versus coverage. There are two distinct regions to the plot. At very low coverage the thickness value is lower than expected. This is due to the layer being effectively inhomogeneous, with the light propagating in the waveguide between distinct regions where a sphere is adsorbed, and regions where no spheres are adsorbed. Above ~17% coverage however a consistent value of the sphere layer thickness is obtained. In this case this is 29.9 ± 0.7 nm ($n = 6$), which compares with the manufacturer quoted sphere dimensions of 24 ± 4 nm for the batch, or 32.4 nm for the volume average measured by dynamic light scattering (DLS), with a number distribution peak at 24.4 ± 2 nm.

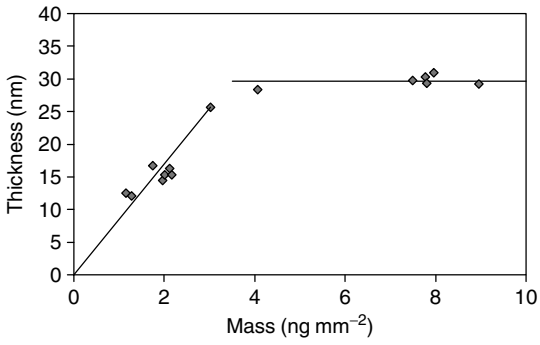

Figure 2. Thickness versus mass (surface excess) of nominally 24-nm polystyrene nanospheres, physisorbed onto an amine chip in PBS, with pH adjusted between pH 2.8 and 4. [Reprinted with permission from Farfield Scientific Ltd.]

3 APPLICATIONS

3.1 Biomolecular Interactions

Many biosensing technologies have been developed for the characterization of biomolecular interactions. The focus being almost exclusively that of determining interaction affinities and binding kinetics, as well as in some more limited cases thermodynamic aspects of the binding interaction. For these, a single binding related response is required. In the interests of brevity we do not focus on these aspects here, but give a few examples where structural measurements provide additional and complimentary information[24] to that which might also be obtained by more conventional biosensor techniques such as SPR.

3.1.1 Molecular Orientation

One structural aspect that can be determined as part of an interaction analysis is molecular orientation. Where the dimensions of a molecule are known, the layer thickness changes measured as part of an analysis can provide information on the orientation and binding site location on a protein.

A model example is the binding of the Fc region of an antibody to protein G. Figure 3 shows the binding response for an IgG3 antibody onto an immobilized protein G layer. The final layer thickness for the antibody of 15.1 nm (when "resolved" to a fixed protein G layer) shows that the antibody is oriented vertically. This is close to the expected antibody dimension for the antibody being captured via the terminus of the F_c domain.

DPI has been used to measure homopolyvalent antibody–antigen interaction kinetics[25] as well as

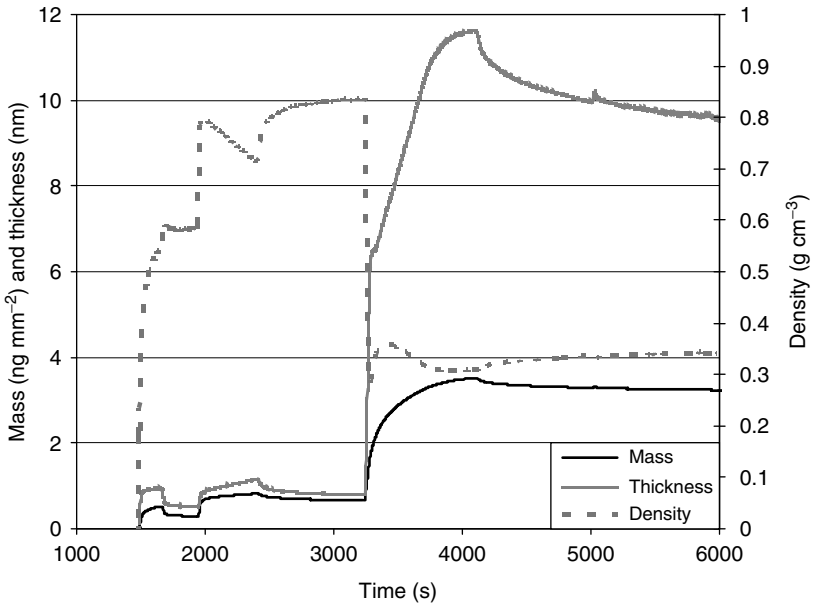

Figure 3. Mass, thickness, and density plot for an oriented IgG3 antibody immobilization. The data was calculated as a single homogeneous layer. The chip is thiol modified, in PBS running buffer. The sequence of sample injections are s-GMBS (1500 s), Protein G (2000 s), and IgG3 antibody (3250 s). [Reprinted with permission from Farfield Scientific Ltd.]

structural changes in polyclonal antibody layers on antigen binding[26,27] where specific and nonspecific interactions can be discriminated on the basis of structural changes.

A demonstration of the ability to use structural measurements to discriminate protein–protein interactions at different binding sites is the interaction of the cell surface protein CD6 with two antibodies specific to different domains on the CD6 molecule. CD6 is involved in regulating T lymphocytes and hence immune regulation. CD6 is a linear molecule containing three scavenger receptor cysteine rich (SRCR) domains, each one approximately 3.5 nm long. The antibodies anti-CD6-D1 and anti-CD6-D3 bind to the first and third domains of CD6 respectively. In this experiment the CD6 is immobilized via a biotinylated two domain spacer (forming a molecule 17 nm long) to a streptavidin surface. The experimentally determined dimensions of the CD6 layer above the streptavidin (14–17 nm) shows that the molecule is oriented predominantly vertically. The structural responses of the two antibodies are very different and summarized subsequently in Figure 4. The antibody binding domain 1 causes a thickness increase and density decrease as it binds to the top of the linear protein array. The antibody to domain 3 however causes the density to increase and the average layer thickness to decrease slightly.

The measured antibody binding results using DPI are fully consistent with the expected binding of the antibody to the CD6 molecule with an orientation also confirmed by DPI.

These results show clearly how structural data obtained as part of a functional measurement can discriminate the interaction of the antibodies with different binding sites on a protein: This data being fully additional to any affinity or kinetic type measurements that might be made, which provide qualitatively different data about the system.

A literature example of the value of structural contributions to biomolecular interactions is the Apolipoprotein E (ApoE) isoprotein-specific interaction with tissue plasminogen activator (tPA), a protein that it modulates as part of the blood clotting cascade.[28] ApoE is an important genetic risk factor for multiple neurological, vascular, and cardiovascular diseases. In this case while the mass of ApoE bound is similar, the thickness of the protein layer is substantially greater for the ApoE3 isoform than either E2 or E4. The protein layer density is also increased considerably after the

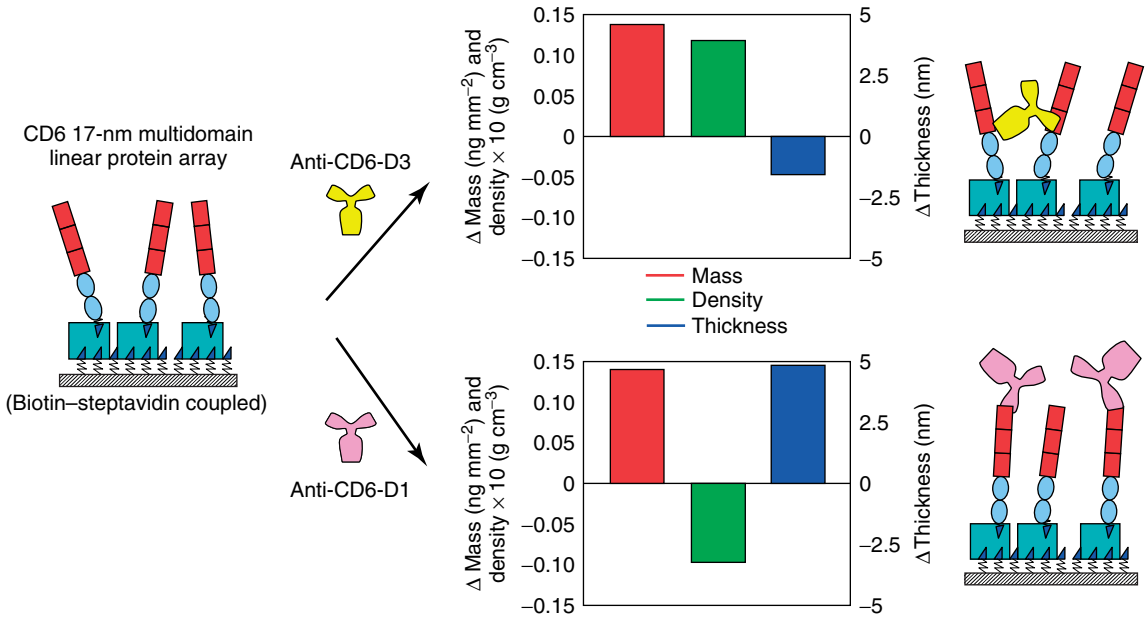

Figure 4. Thickness mass and density changes for CD6 complex–antibody interactions and schematic representation of the binding event. [Reprinted with permission from Farfield Scientific Ltd.]

addition of ApoE2 whereas density was decreased with addition of ApoE3 or E4. These measured differences also reflect physiologically observed differences between the different phenotypes. ApoE has been linked to outcome and survival following acute injury of the central nervous system as well as the cardiovascular system.

3.2 Lipid and Membrane Studies

3.2.1 Introduction

Many important biological processes such as intra- and intercellular signaling occur at membrane interfaces. Given that such processes are involved in many disease mechanisms, including cancer, the study of active components in the membrane is an area of intense research activity in both the academic sector and the biotechnology and pharmaceutical industries.[29] Cellular membranes are complex, the bulk of the membrane "matrix" being made up of phospholipids assembled into a bilayer structure. The membrane contains a range of additional components such as cholesterol and proteins. The latter provide specific functions such as transporting molecules across the membrane (e.g., signaling).[30]

The amphiphilic nature of phospholipids drives them to self assemble into structures which minimize hydrophobic–hydrophilic interactions. Thus in the cell membrane the lipids form a bilayer in which the tails of the lipid molecules are adjacent to each other leaving the hydrophilic head groups facing out on either side of the layer. Lying within this layer are the cholesterol and other components of the membrane.

A wide range of studies have been carried out using biomimetic systems using single or mixed lipid systems with and without additional components such as cholesterol. The preparation of lipid structures is far from straightforward[31–33] as a wide range of structural variation has been observed in the preparation of in vitro lipid systems. Depending upon the exact conditions of preparation, lipid cakes, rods, and/or vesicles may be formed in addition to supported bilayer structures. It is often difficult to assign, without ambiguity, the particular structures which have been generated in a given experiment. The ability to probe both the dimensions and the density of layer structures obtained using DPI can help to reduce this ambiguity.

Using simple geometric modeling it is possible to predict the likely surface characteristics that will be obtained when, for example, single bilayer wall (unilamellar) vesicles are deposited on a surface as opposed to double bilayer wall (bilamellar) vesicles are deposited on the waveguide surface. Thus the most likely lipid structures formed on the surface of the waveguide can be readily identified.

Typical experimental protocols involve the hydration of the appropriate lipid/s followed by the formation of vesicles by sonication/surfactant depletion or extrusion. The resultant solutions are then flowed over the waveguide surface and the resultant surface layers measured. The waveguide surface was either used as is or modified as required. Hybrid bilayer membranes (HBM) can also be produced by flowing solutions of vesicles over waveguide surfaces which have been modified with for example, octadecylsilanes or decanoic acid surface.[34] Whatever the selected method, the multiparametric measurement of the layers formed can be monitored in real time and related to the most likely structures obtained.

3.2.2 Structures–Lipid Vesicle Structures

DPI has been used to study a wide range of phospolipids. 1,2-distearoyl-*sn*-glycerol-3-phosphatidic acid (DSPA) will be used to demonstrate the utility of DPI and simple modeling to investigate lipid structures. Free standing lipid vesicles can be simply constructed on a waveguide surface by perfusing lipid vesicle solutions and an example is given in Figure 5.

Lipid vesicles may be formed from multiple bilayer structures, being unilamellar, bilamellar, trilamellar, or greater. It is however difficult to elucidate the number of lamellae within the vesicle, often requiring the use of cryotransmission electron microscopy to unambiguously determine the structure. The dimensions and density of the layers formed provides information on the likely structures obtained. Taking the example of DSPA, the layer characteristics can be compared with calculated layer characteristics in order to elucidate the likely vesicle structures can be demonstrated. In Table 2 the observed characteristics of the DSPA lipid vesicle layer are compared with the predicted characteristics. It is clear that the layer characteristics are most consistent with a multilamellar vesicle which is effectively a "solid onion" structure.

3.2.3 Liposome–Peptide Interactions

DPI has been used to study a number of peptides associating with membranes, including antimicrobial peptide V4, and duramycin. Taking the example of melittin, a small peptide which is a component of bee venom. It is known to disrupt certain

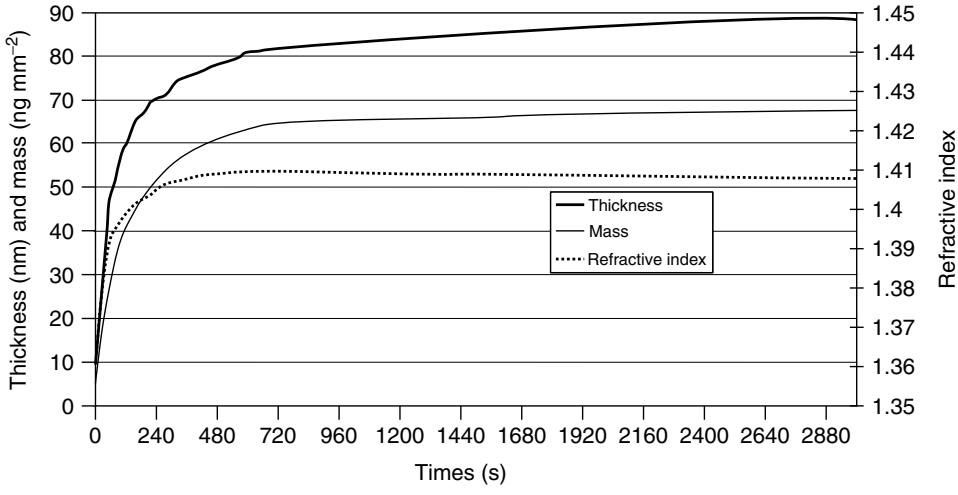

Figure 5. Thickness, refractive index, and mass of a layer of DSPA liposomes added to an unmodified, silicon oxynitride surface at a flow rate of 25 µl m^{-1} in PBS. [Reproduced from Popplewell et al.[35]. © BBA Membranes.]

Table 2. Calculated and observed thickness and refractive-index values for a spherical DSPA multilamellar liposome (in this case the lamellae exceed six in number and there is no distortion)

	Number of lamellae[(a)]	Thickness (nm)	Refractive index	Longitudinal axis (nm)	Equatorial axis (nm)
Observed (DLS)		79 (±20)	n/a	87	n/a
Observed (DPI)		87 (±9)	1.405	87	n/a
Calculated	1	87	1.355	87	87
	3	87	1.384	87	87
	6	87	1.396	87	87
	Solid	87	1.404	87	87

[(a)] Assuming 100% layer coverage.
[Reprinted with permission from Farfield Scientific Ltd.]

classes of lipid structure. The mechanism by which this disruption occurs is still a matter of debate and DPI has been used to examine aspects of melittin–lipid bilayer interactions. Melittin is amphipathetic, the n-terminus carrying hydrophobic amino acid residues while the c-terminus carries predominantly hydrophilic residues and is highly positively charged (carrying 6 positive charges). The influence of melittin on a 1,2-dioleoyl-sn-glycero-3-phosphocholine (DOPC) lipid vesicle layer is shown in Figure 6. Melittin was perfused over the stable vesicle layer commencing at 19 760 s. Initially the layer is seen to increase in mass, density, and dimensions as melittin binds to the external surface of the vesicles. During the initial 30 s the layer dimension holds at circa 20 nm which is consistent with the maintained integrity of the vesicles. However after 30 s there is a rapid decrease in the dimensions and mass of the layer and a concomitant increase in the density. The final dimensions of the layer are consistent with a single supported bilayer on the surface of the waveguide. Further insights into the mechanism of action were elucidated by examining layer structure change obtained with lipid vesicles constituted with different lipids (varying the charge and TM)

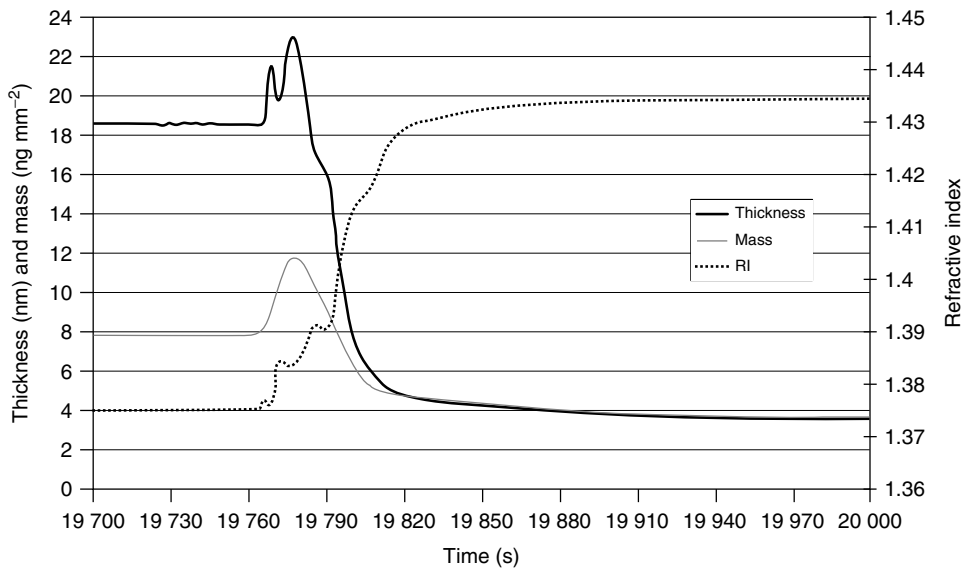

Figure 6. The effect of an injection of melittin (0.5 mg ml^{-1}) on the dimensions of an immobilized layer of DOPC liposomes. On addition of melittin there is an initial increase in refractive index, mass, and thickness as the melittin associates with DOPC, followed by a rapid decrease in both mass and thickness as the liposome ruptures. [Reproduced from Popplewell et al.[35]. © BBA Membranes.]

and examining the stoichiometry which leads to vesicle rupture (found to be approximately 1 melittin:6 outer hemilayer lipid molecules).[35]

3.3 Protein–Small Molecule Interactions

3.3.1 Introduction

The measurement of interactions of proteins with small molecules (compounds and small peptides under 1000 Da) is an area that is both challenging and of significant commercial interest. The main driving force is from the drug discovery process, where measurements can support many areas from target identification, ligand fishing, assay development, and lead selection through to early absorption, distribution, metabolism, excretion (ADME) and manufacturing quality control.[36] Measurements in these areas require a high degree of sensitivity and can be greatly affected by changes in buffer condition (drug compounds often being stored in dimethyl sulfoxide (DMSO)).

There are two aspects in which structural measurement in conjunction with probes of molecular function can be obtained with DPI measurements. This is in the direct measurement of conformational change related to a binding process, and the other is a structurally significant binding event.

The first of these may be demonstrated with the model system streptavidin–biotin,[26] while the second is exemplified by the binding of cortisol by anticortisol. In both cases, changes in the average layer structure (thickness and RI) can be related to a particular binding event. This provides a method for the characterization of small (drug) molecule interactions, where a plot of the percentage density change in the protein molecule versus the percentage thickness change can act as a classification method for a particular binding mode that uses the structural changes that a molecule elicits rather than (or as well as) the more conventional extent versus affinity plot (cf. Figure 4 in Ref. 36).

3.3.2 Antihydrocortisone–Hydrocortisone Interaction

The affinity plot for a hydrocortisone antibody based on thickness change is shown in Figure 7(a). These can be plotted from RI or density as well as mass changes. The antibody layer had been immobilized in an oriented manner using protein G, and the dimensional measurements confirmed this (Antibody layer Th = 15.1 nm).

The size/density plot for this interaction is shown in Figure 7(b). Here the thickness increases and the density decreases. This is a structurally significant response giving a large structural change. The antibody is immobilized in an oriented fashion on protein G, and the response reflects the hydrocortisone binding at the terminal binding sites on the F_{ab} fragments at the top of the oriented antibody. The figure shows all the concentration data, which lie on the same radial line. This shows that in principle the structural effect of a small molecule can be determined from a single concentration sample. For comparison note the response of streptavidin to biotin, Figure 7(c), where the tight binding results in a conformational tightening which is also born out by X-ray data.[26]

3.4 Metal Ion Interactions

3.4.1 Introduction

Many proteins have their function mediated by concentrations of cations in solution; so the body controls levels of protons, sodium, and potassium across cell membranes. Similarly, divalent cations such as calcium modulate the activity of many different proteins. Measuring the interactions of specific ions with proteins is a challenging task, as the mass changes are often vanishingly small. Often, structural changes are more significant, but again prove difficult to identify.

DPI has been used to measure the structural and mass changes of a number of proteins as a function of metal ion concentration. These include calmodulin (Ca^{2+}), prion protein (Cu^{2+}, Mn^{2+}, Zn^{2+}, Fe^{2+}, Mg^{2+}, Ni^{2+}), human serum albumin, HSA (Cu^{2+}, Ni^{2+}), BSA (Ni^{2+}), β-Amyloid (Cu^{2+}, Mg^{2+}). Here as an example we show the response of tissue transglutaminase, which binds calcium ions.[37]

3.4.2 Transglutaminase–Calcium Ion Binding

Transglutaminases are catalysts involved in the post-translational modification of proteins, forming isopeptide bonds at glutamine residues. This

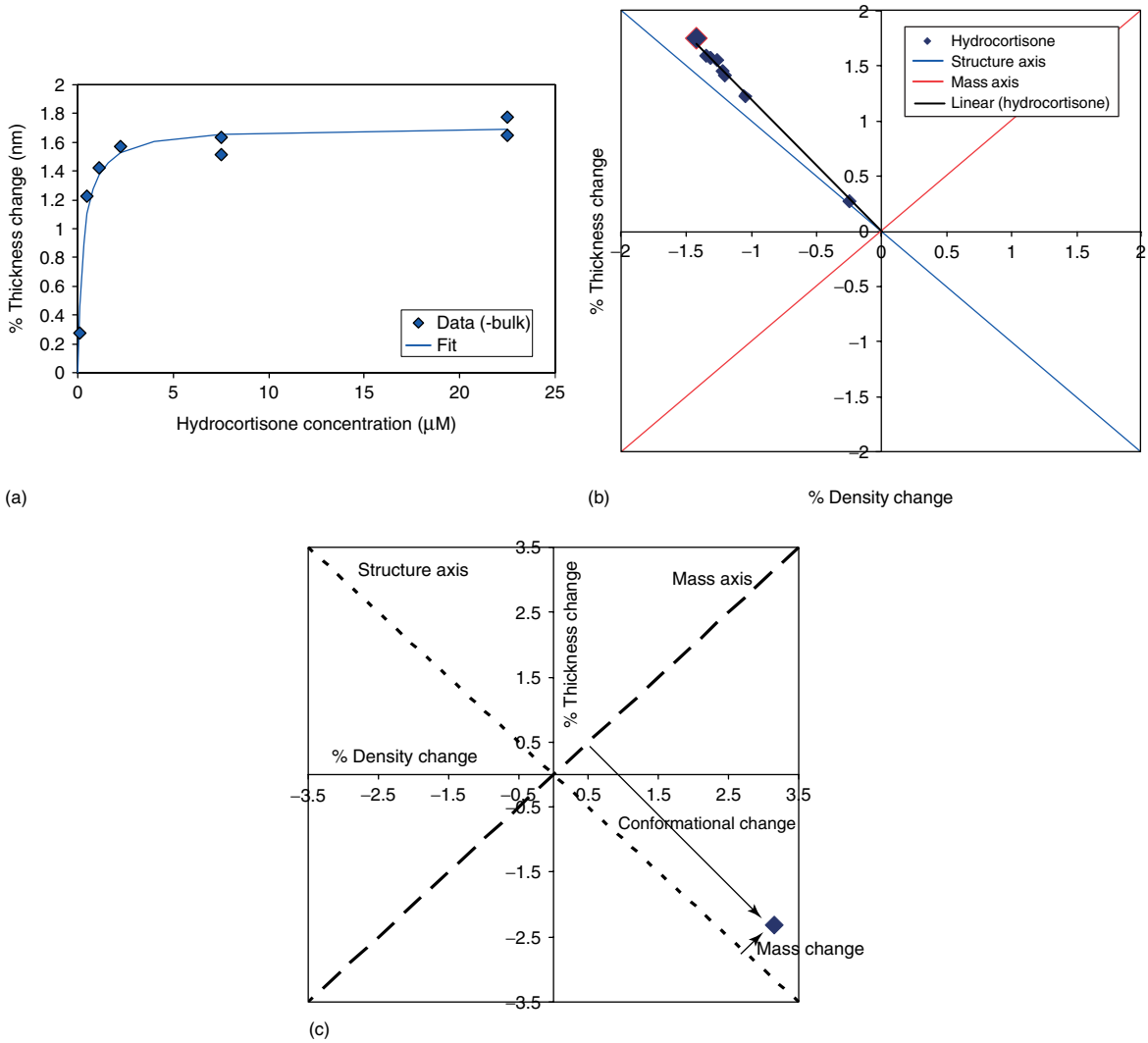

Figure 7. (a) Binding curve for hydrocortisone and antihydrocortisone. Affinity fit 0.28 μM. The antibody was immobilized on a thiol chip via s-GMBS and protein G. The hydrocortisone was diluted from a stock DMSO solution, and the response corrected for the bulk RI contribution from the DMSO. (b) Size/density plot for hydrocortisone/antihydrocortisone interaction. The individual points correspond to concentration injections of 0.1–22.5 μM hydrocortisone. (c) Size/density matrix plot of the conformational change for streptavidin binding biotin (SA immobilized on a biotinylated amine chip). [Reprinted with permission from Farfield Scientific Ltd.]

activity has been shown to be modulated by calcium and guanosine 5′-triphosphate (GTP). This modulation is thought to be related to *putative* conformational changes induced by the modulators. Indirect analysis using shallow angle neutron scattering (SANS) and shallow angle X-ray scattering (SAXS) and circular dichroism spectroscopy have suggested that there is a significant increase of 0.8 nm in the gyration radius of the protein on binding calcium suggesting a significant broadening of the protein structure on binding. Efforts to elucidate conformational changes directly from crystallographic data have not been successful. Reports on optical measurements of transglutaminase on the addition of calcium have also been reported in which anomalies in the

expected responses have been attributed to likely conformational changes in the protein on binding calcium.

Using DPI it has been possible to measure the conformational changes associated with calcium binding directly. The protein was immobilized to an amine functionalized sensor surface via free external amine groups using BS^3. A thickness increase of 5 nm was observed which demonstrates that the disc shaped molecule (approximately 15 nm in diameter and 5 nm thick) had been immobilized face parallel to the chip surface as might be expected. Once the protein surface had been created, it was challenged with different concentrations of calcium chloride and chloride mol equivalents of sodium chloride. On binding calcium, the transglutaminase undergoes significant conformational changes with a thickness contraction of 0.4 nm. The RI changes as a function of calcium concentration are shown in Figure 8. The experiment can be performed and analyzed in a number of ways. The data in Figure 8 is obtained by analyzing a single channel, and using the sodium injections as a control for changes due to ionic strength and bulk RI. The affinity constant has been calculated to be 1.16 mM which compares well with the range of literature values for the interaction which span the range 0.2–3.0 mM. An alternative method of data analysis uses the data obtained on the control channel (a surface treated in the same way, but without the protein) as a control subtraction.[37] This produces a very similar result with affinity calculated at 0.95 mM.

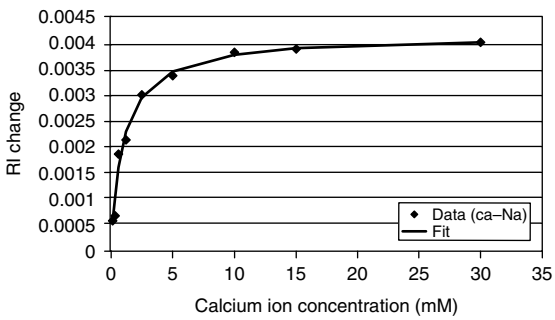

Figure 8. Plot of RI change as a function of calcium ion concentration. The data has been corrected for ion charging and bulk refractive-index effects by subtraction of the response from NaCl injections at the same ionic strength. Calcium ion affinity 1.16 mM. [Reprinted with permission from Farfield Scientific Ltd.]

This clearly suggests that the structural changes observed are directly related to the binding of calcium.

3.5 Biomolecular Stability and Structure

3.5.1 Introduction

Understanding biomolecular structure and stability at surfaces is important in a wide range of applications from the optimization and quality control of diagnostic devices to the functionalization of surfaces of materials such as contact lenses which are prone to biofouling to the preparation of medical implants which are in contact with the body for extended periods of time. For biocompatible devices, the fate of protein structure at the surface is critical in terms of the viability of medical devices and their ability to function normally. In many cases the forces which proteins are exposed to at surfaces are sufficient to disrupt the tertiary and quaternary structure leading to compromised functional capability, the mobilization of the immune system, and ultimately to rejection. In the case of diagnostic or sensing devices, the structure of proteins and other molecules at a surface will have a significant effect on the device's functionality.

DPI has been used to examine a number of key aspects in the determination of the fate of protein at surfaces under different environmental conditions.

3.5.2 Surface Development/immobilization

The orientation of antibodies on a solid surface has a significant effect on the overall activity of the molecule. Antibodies have two "arms" (see Figure 9a) which are implicated in the capture of antigens and if these are too restricted either as a consequence of lying on the surface or due to steric crowding of neighboring molecules the activity of the antibody will be compromised or extinguished altogether. Therefore obtaining information on the orientation of immobilized antibodies and factors effecting the orientation during the immobilization process are of great interest.

A study of such processes has been undertaken using DPI. A range of immobilization strategies were employed and the resulting structures

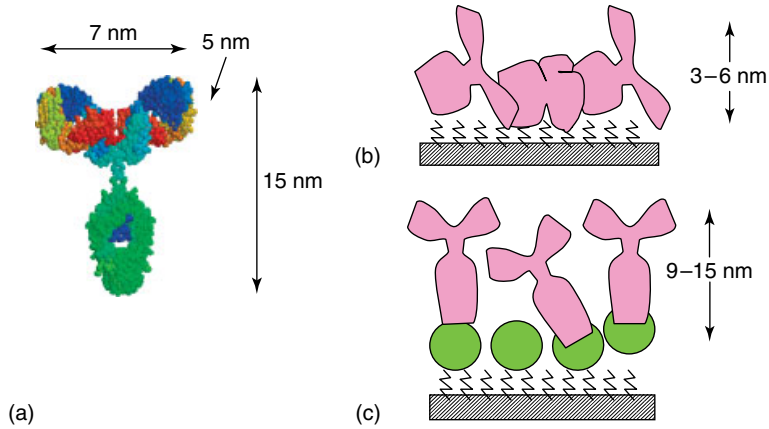

Figure 9. (a) Molecular structure of an IgG3 antibody with approximate dimensions; (b) Typical surface obtained when using amine coupling chemistry (inactive); (c) Typical surface obtained when using protein G coupling strategy (active). [Reprinted with permission from Farfield Scientific Ltd.]

and activities measured. Typically, when crude immobilization strategies are used layer dimensions of 7 nm or less are observed. Antibody layers which are 6 nm or less are on the whole inactive or severely compromised. Generally when antibody layers have dimensions which are greater than 7 nm (and from mass calculations have an appropriate area per molecule to indicate a monolayer) the antibody is likely to be active.

Examples of antibody layers obtained and their activities post immobilization are provided in Table 3.

Similarly, DPI has also been used for assessing immobilization strategies for DNA sensing surfaces.[38,39] This is a particularly challenging area due to the high charge on the DNA backbone making accessible orientation of the DNA molecule difficult to achieve.

3.5.3 Environmental Effects

Proteins undergo substantial structural changes as a consequence of their local environment. Some

Table 3. Examples of antibody immobilization strategies, dimensions of layers obtained, and resulting activities to respective antigens

Antibody	Type	Immobilization	Antibody layer (nm)	Activity	Antigen (MWt)	Δ Thickness (nm)
Ovalbumin		$-NH_2$, BS^3	3.3	Inactive	5000	None
HSA	IgG1	$-NH_2$, BS^3	6.4	Active $\ll$ 1:1	67 000	Positive
Bi-ProBNP	Poly	$-NH_2$, SA, s-NHS-LC Biotin,	6.7	Active 1:1	8000	Negative
BSA	IgG1	$-NH_2$, BS^3, Protein G	6.0	Inactive	66 000	None
Cortisol (1)	IgG3	$-NH_2$, BS^3, Protein G	9.0	Active 2:1	362	Positive
Cortisol (2)	IgG3	−SH, s-GMBS, Protein G	15.1	Active 2:1	362	Positive
PrP	IgG2a	−SH, s-GMBS, Protein G	11.2	Active 1:6	24 000	Positive/none

HSA: human serum albumin; BSA: bovine serum albumin; BS^3:bis(sulphosuccinimydyl) suberate; ProBNP: precursor of brain natriuretic peptide; PrP: prion protein.
[Reprinted with permission from Farfield Scientific Ltd.]

Table 4. pH cycling profile low-high-low with lysozyme concentration fixed at 1.0 g dm^{-3}

pH	Layer thickness (Å ± 1)	Refractive index (±0.001)	Mass loading (mg m^{-2} ± 0.05)	Area per molecule ($Å^2$)	Protein volume fraction (±0.001)
4	25	1.401	0.89	2733 ± 100	0.343 ± 0.001
7	49	1.443	2.91	832 ± 50	0.568 ± 0.001
4	37	1.431	2.01	1208 ± 60	0.520 ± 0.001

[Reprinted with permission Freeman et al.[41] © 2004 American Chemical Society.]

changes will be in order to render the protein active/inactive such as the binding of specific metal ions, changes in pH and so on, while other changes will be irreversible (denaturation) typically as a consequence of excessive heat. Studies of structural changes as a consequence of environmental changes have been undertaken using DPI, such as the pH dependent adsorption of BSA.[21]

3.5.4 Lysozyme

Lysozyme adsorption at the silica water interface is another extensively investigated model system. The behavior of the protein at the interface has been studied primarily using neutron reflection techniques and ellipsometry. These studies were, in the main carried out using pure silicon dioxide surfaces[40] whereas the waveguide surfaces used in typical DPI experiments are lightly doped with nitride. In addition DPI experiments were carried out using a flow through cell arrangement rather than the static fluidic systems preferred by previous experimenters. Despite these differences, correlations between data from these analytical techniques are extremely good.[41]

The lysozyme was prepared in two pH buffer solutions and at the desired concentrations and flowed over the waveguide surface at a constant flow rate (50 µl min^{-1} per channel). The layer characteristics obtained were measured using DPI in real time (measurement frequency 0.1 s) and compared with available published data.

At pH 4 there is a considerable amount of positive charge on the lysozyme molecules and the adlayers obtained are relatively sparse, the molecules probably lying with their short axes normal to the mildly negatively charged waveguide surface. At pH 7 the layers obtained at low concentration also appear go down on to the surface short axis normal but at higher concentrations appear to reorient themselves long axis normal to the waveguide surface. This change in behavior is probably due to the reduced electrostatic repulsions at higher pH between neighboring lysozyme molecules on the waveguide surface. Changes in the adlayer structure when the pH is cycled between pH 4 and 7 are shown in Table 4.

3.5.5 Protein Surfactant Structures

The behavior of surfactants used to prevent protein aggregation (Tween™) have been studied at the waveguide surface. Comparing the properties of the Tween® series we find that the head groups are large relative to the hydrophobic tail groups and are of a similar size. Moving from Tween® 20 through 60 the saturated alkyl tails extend in length while Tween® 80 has a single carbon–carbon double bond in it (increasing the molecular fluidity).[42] It can be seen from Figure 10 that the thickness of the adlayer is directly proportional to the hydrophilicity of the molecules involved. Thus, regardless of the size of the molecule involved,

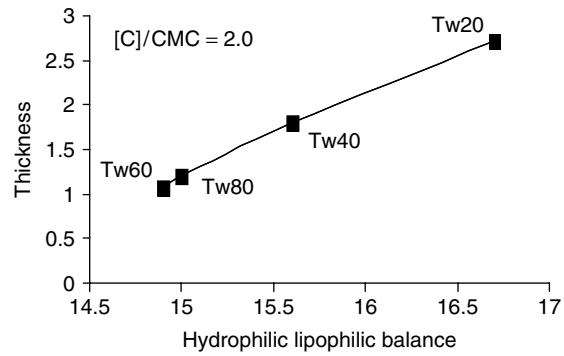

Figure 10. Thickness versus hydrophilic lipophilic balance (HLB) for the series of Tween™ 20–80 surfactants at [C]/CMC of 2.0. [Reprinted with permission from Farfield Scientific Ltd.]

it appears to be the energetics of solvation in water that ultimately determine the structures of the adlayers on the surface of the waveguide. Thus the most hydrophilic molecule Tween® 20 forms the thickest and most diffuse adlayer while Tween® 80 forms the thinnest densest adlayer.

4 FUTURE DEVELOPMENTS

The optical waveguide device can be considered to be an optical bench. As such, a wide variety of optical experiments can, in principle, be carried out either sequentially or, preferentially, simultaneously. Rather than listing the variety of such experiments, for the sake of brevity, just one extension to the DPI technique will be briefly discussed here.

4.1 Waveguide Extinction Coefficients

All of the data discussed to date has related to the measurement of changes in phase of light propagating through the sensing waveguide relative to the underlying reference waveguide as measured by changes in the position of interference fringes. A relative measure of the light lost from the sensing waveguide can be made quite simply by measuring the contrast of the interference fringe image (the losses). The contrast provides a relative measurement of the amount of light transmitted through the sensing waveguide compared to that transmitted through the reference waveguide. Information on losses enables inferences to be made regarding the nature of structures within the layer such as nucleated versus stochastic packing of bodies within the layer. The measurement of extinction coefficients and their interpretation is actively being developed and a full analytical solution for waveguide losses has been developed which it is anticipated will provide yet further information on the structure and arrangement of proteins and other biologically relevant molecules on the surface.

During this development a special case was identified with respect to waveguide losses. It has been observed that losses from the waveguide structure increase substantially when crystallization occurs. This is distinct from aggregation, precipitation, and other nonordered solid-state phases which do not lead to the same dramatic losses. Early experimental data was obtained using the model protein lysozyme. During the early stages of the crystallization process it was possible to measure the characteristics of the layer structure formed on the waveguide surface. These experiments suggested that, assuming expitaxial growth, that the crystallization could be detected when groups of around 30 molecules or so were present. This would suggest that this approach is capable of identifying the very early stages of crystallization and possibly to nucleation event itself. Given the insensitivity to other solid-state phases, it has been possible to determine crystallization even in the presence of precipitates.

A range of proteins have been studied and while the initial conditions for crystallization vary considerably all have shown similar characteristics during the course of crystallization. Preliminary studies using nondiffracting crystals and salt crystals suggest that it might be possible to elucidate between these classes using such waveguide techniques. If this proves to be the case then it should be possible to substantially enhance the productivity of protein structure determination for which the production of diffraction quality protein crystals is the bottleneck.

4.2 Chip Functionalization

Chip functionalization is a critical area for tagless biosensor systems. The immobilization of proteins on surfaces in a manner which it is both biologically relevant and does not result in excessive nonspecific binding is important in the reduction of ambiguity of experimental results. One approach to this problem is to use biomimetic surfaces such as carbohydrates.

4.2.1 Carbohydrate Chips

Preliminary work attaching keratin sulfate (KS), a 7 kDa oligosaccharide to waveguide surface has demonstrated high specificity to proteins binding KS sequences compared to those which do not (e.g., lactoferin binds strongly while concanavalin A does not). Similarly encouraging results have been obtained using condroitin sulfate (CS) and heparin sulfate (HS). These surfaces show a high level of nonspecific binding which appear to resist the physisorption of BSA even at relatively high

concentrations (0–2 mg ml^{-1}). The flexibility of the chemistries which can be deployed and their relatively high activities on waveguide surfaces suggest that in the future these surfaces may offer very high level of performance for tagless biosensor systems.

5 CONCLUSIONS

Dual polarization interferometry is a highly sensitive surface analytical technique that has been used for measuring the structure, orientation, and functionality of biological and other layers at the liquid–solid interface. The potential areas of application are many and varied; however they share the common theme of providing a greater level of understanding of the complex processes of molecular arrangement and interactions. The technique relies on classical optics which is well understood and provides dimensional information to a very high resolution (typically better than 0.01 nm) and mass loadings to a resolution of around 100 fg mm^{-2}. It is possible not only to detect interactions between large proteins and small molecules but also to quantify them and to determine stoichiometries. Furthermore the technique shows promise for further development to provide information beyond that obtained from layer thickness and RI.

ACKNOWLEDGMENTS

The authors would like to thank Prof. David Fernig (Liverpool University), Dr David Cullen, Dr Kal Karim, and Dr Judith Taylor (Cranfield University), Prof. Jian Lu (Manchester University), and Prof. Neil Barclay (Oxford University) for their experimental expertise and advice. We also gratefully acknowledge the experimental skills and diligence of Dr Jonathan Popplewell, Dr Louise Peel, Dr Mark Gostock (Farfield Scientific Ltd.) who undertook much of the experimental work described. We would also like to thank Dr Gerry Ronan, Dr Simon Carrington, and Dr Kathryn Chapman (Farfield Scientific Ltd.) for helpful discussions on the most appropriate ways to describe some of the physical concepts utilized by DPI and the BBSRC for research funding.

REFERENCES

1. H. Arwin, Ellipsometry on thin organic layers of biological interest: characterization and applications. *Thin Solid Films*, 2000, **48**, 377–378.
2. R. M. A. Azzam and N. M. Bashara, *Ellipsometry and Polarised Light*, North Holland, Amsterdam, 1977.
3. P. M. Nellen, K. Tiefenthaler, and W. Lukosz, Input grating couplers as biochemical sensors. *Sensors and Actuators*, 1988, **15**, 285.
4. L. Guemouri, J. Ogier, and J. J. Ramsden, Optical properties of protein monolayers during assembly. *Journal of Chemical Physics*, 1998, **109**, 3265.
5. Z. Salamon and G. Tollin, Optical anisotropy in lipid bilayer membranes: coupled plasmon-waveguide resonance measurements of molecular orientation, polarizability, and shape. *Biophysical Journal*, 2001, **80**, 1557.
6. G. H. Cross, A. A. Reeves, S. Brand, M. J. Swann, L. L. Peel, N. J. Freeman, and J. R. Lu, The metrics of surface adsorbed small molecules on the Young's fringe dual-slab waveguide interferometer. *Journal of Physics D: Applied Physics*, 2004, **36**, 74.
7. B. Liedberg, C. Nylander, and I. Lundstrom, Surface plasmon resonance for gas detection and biosensing. *Sensors and Actuators*, 1983, **4**, 299.
8. G. Ramsay, *Commercial Biosensors*, John Wiley & Sons, 1998.
9. Z. Salamon, H. A. Macleod, and G. Tollin, Coupled plasmon-waveguide resonators: a new spectroscopic tool of probing film structure and properties. *Biophysical Journal*, 1997, **73**, 2791.
10. E. Kretschmann, Die Bestimmung optischer Konstanten von Metallen durch Anregung von Oberflachenplasmaschwingungen. *Zeitschrift fur Physik*, 1971, **241**, 313.
11. Z. Salamon, H. A. Macleod, and G. Tollin, Surface plasmon resonance spectroscopy as a tool for investigating the biochemical and biophysical properties of membrane protein systems. I: Theoretical principles. *Biochimica Et Biophysica Acta*, 1997, **1331**, 117.
12. J. Voros, J. J. Ramsden, G. Csucs, I. Szendro, S. M. DePaul, M. Textor, and N. D. Spencer, Optical grating coupler biosensors. *Biomaterials*, 2002, **23**, 3699.
13. W. Lukosz and K. Tiefenthaler, Sensitivity of integrated optical grating and prism couplers as (bio)-chemical sensors. *Sensors and Actuators*, 1988, **15**, 273.
14. E. K. Mann, Evaluating optical techniques for determining film structure: optical invariants for anisotropic dielectric thin films. *Langmuir*, 2001, **17**, 5872.
15. R. G. Heideman and P. V. Lambeck, Remote opto-chemical sensing with extreme sensitivity: design, fabrication and performance of a pigtailed integrated optical phase-modulated Mach–Zehnder interferometer system. *Sensors and Actuators*, 1999, **B61**, 100–127.
16. G. H. Cross, Y. T. Ren, and N. J. Freeman, Young's fringes from vertically integrated slab waveguides: applications to humidity sensing. *Journal of Applied Physics*, 1999, **86**, 6483–6488.
17. M. B. Huglin, *Light Scattering from Polymer Solutions*, Academic Press, New York, 1972.
18. J. Wen and T. Arakawa, Refractive index of proteins in aqueous sodium chloride. *Analytical Biochemistry*, 2000, **280**, 327–329.

19. J. A. de Feijter, J. Benjamins, and F. A. Veer, Ellipsometry as a tool to study the ad-sorption of synthetic and biopolymers at the air-water interface. *Biopolymers*, 1978, **17**, 1759–1772.
20. S. Lin, C.-K. Lee, Y.-M. Wang, L.-S. Huang, Y.-H. Lin, S.-Y. Lee, B.-C. Sheu, and S.-M. Hsu, Measurement of dimensions of pentagonal doughnut-shaped C-reactive protein using an atomic force microscope and a dual polarisation interferometric biosensor. *Biosensors and Bioelectronics*, 2006, **22**(2), 323–327.
21. N. J. Freeman, L. L. Peel, M. J. Swann, G. H. Cross, A. Reeves, S. Brand, and J. R. Lu, Real time, high resolution studies of protein adsorption and structure at the solid-liquid interface using dual polarisation interferometry. *Journal of Physics: Condensed Matter*, 2004, **16**, S2493–S2496.
22. G. H. Cross, A. Reeves, S. Brand, J. F. Popplewell, L. L. Peel, M. J. Swann, and N. J. Freeman, A new quantitative optical biosensor for protein characterisation. *Biosensors and Bioelectronics*, 2003, **19**, 383–390.
23. T. Halthur, P. Claessen, and U. Elofsson, Immobilization of enamel matrix derivate protein onto polypeptide multilayers. Comparative in situ measurements using ellipsometry, quartz crystal microbalance with dissipation, and dual-polarization interferometry. *Langmuir*, 2006, **22**(26), 11065–11071.
24. G. Thibault, J. Yudin, P. Wong, V. Tsitrin, R. Sprangers, R. Zhao, and W. A. Houry, Specificity in substrate and cofactor recognition by the N-terminal domain of the chaperone ClpX. *Proceedings of the National Academy of Sciences of the United States of America*, 2006, **103**(47), 17724–17729.
25. S. Lin, C.-K. Lee, Y.-H. Lin, S.-Y. Lee, B.-C. Sheu, J.-C. Tsai, and S.-M. Hsu, Homopolyvalent antibody-antigen interaction kinetic studies with the use of a dual polarisation interferometric biosensor. *Biosensors and Bioelectronics*, 2006, **22**(5), 715–721.
26. M. Swann, L. Peel, S. Carrington, and N. Freeman, Dual polarisation interferometry: an analytical technique to measure changes in protein structure in real time, to determine the stoichiometry of binding events and to differentiate between specific and non-specific interactions. *Analytical Biochemistry*, 2004, **329**, 190–198.
27. M. Swann, N. Freeman, S. Carrington, G. Ronan, and P. Barrett, Quantifying structural changes and stoichiometry of protein interactions using size and density profiling. *Letters in Peptide Science*, 2003, **10**, 487–494.
28. S. Biehle, J. Carrozzella, R. Shukla, J. Popplewell, M. Swann, N. Freeman, and J. Clark, Apolipoprotein E isoprotein specific interactions with tissue plasminogen activator. *Biochimica Et Biophysica Acta-Molecular Basis of Disease*, 2004, **1689**, 244–251.
29. G. C. Terstappen and R. Angelo, In silico research in drug discovery. *Trends in Pharmacological Sciences*, 2001, **22**, 23–26.
30. M. Cascio and R. S. Rapaka, Structural biology and structural genomics/proteomics. *Journal of Peptide Research*, 2002, **60**, 307–311.
31. B. A. Lewis and D. M. Engelman, Surface areas and volumes of DPPC by X-ray scattering. *Journal of Molecular Biology*, 1983, **166**, 211–217.
32. M. Seitz, E. Ter-Ovanesyan, M. Hausch, C. K. Park, J. A. Zasadzinki, R. Zentel, and J. N. Israellachvili, Formation of tethered supported bilayers by liposome fusion onto lipopolymer monolayers promoted by osmotic stress. *Langmuir*, 2000, **16**, 6067–6070.
33. J. Majewski, J. Y. Wong, C. K. Park, M. Seitz, J. N. Israelachvili, and G. S. Smith, Structural studies of polymer-cushioned lipid bilayers. *Biophysical Journal*, 1998, **75**, 2363–2367.
34. C. Terry, J. Popplewell, M. Swann, N. Freeman, and D. Fernig, Characterisation of membrane mimetics on a dual polarisation interferometer. *Biosensors and Bioelectronics*, 2006, **22**(5), 627–632.
35. J. F. Popplewell, M. J. Swann, N. J. Freeman, C. McDonnell, and R. Ford, Quantifying the effects of melittin on liposomes. *Biochimica Et Biophysica Acta-Biomembranes*, 2007, **1768**(1), 13–20.
36. M. A. Cooper, Optical biosensors in drug discovery. *Nature Reviews Drug Discovery*, 2002, **1**, 515–528.
37. K. Karim, J. D. Taylor, D. C. Cullen, M. J. Swann, and N. J. Freeman, Measurement of conformational changes in the structure of transglutaminase on binding calcium ions using optical evanescent dual polarisation interferometry. *Analytical Chemistry*, 2007, **79**(8), 3023–3031.
38. H. Berney and K. Oliver, Dual polarization interferometry size and density characterisation of DNA immobilisation and hybridisation. *Biosensors and Bioelectronics*, 2005, **21**, 618–626.
39. B. Lillis, M. Manning, H. Berney, E. Hurley, A. Mathewson, and M. Sheehan, Dual polarisation interferometry characterisation of DNA immobilisation and hybridisation on a silanised support. *Biosensors and Bioelectronics*, 2006, **21**, 1459–1467.
40. J. R. Lu and R. K. Thomas, Nuetron of reflection from wet interfaces. *Journal of the Chemical Society, Faraday Transactions*, 1998, **94**(8), 995.
41. N. J. Freeman, L. L. Peel, M. J. Swann, and J. R. Lu, Lysozyme adsorption studies at the silica-water interface using dual polarisation interferometry. *Langmuir*, 2004, **20**, 1827–1832.
42. L. Stryer, *Biochemistry*, 4th Edn, W. H. Freeman, New York, 1995.